

Dispersive Bottleneck Delaying Thermalization of Turbulent Bose-Einstein Condensates

Giorgio Krstulovic and Marc Brachet

*Laboratoire de Physique Statistique de l'Ecole Normale Supérieure, associé au CNRS et aux Universités Paris VI et VII,
24 Rue Lhomond, 75231 Paris, France*

(Received 26 July 2010; revised manuscript received 10 January 2011; published 16 March 2011)

A new mechanism of thermalization involving a direct energy cascade is obtained in the truncated Gross-Pitaevskii dynamics. A long transient with partial thermalization at small scales is observed before the system reaches equilibrium. Vortices are found to disappear as a prelude to final thermalization. A bottleneck that produces spontaneous effective self-truncation and delays thermalization is characterized when large dispersive effects are present at the truncation wave number. Order of magnitude estimates indicate that self-truncation takes place in turbulent Bose-Einstein condensates. This effect should also be present in classical hydrodynamics and models of turbulence.

DOI: 10.1103/PhysRevLett.106.115303

PACS numbers: 67.25.dj, 03.75.Kk, 42.65.Sf, 47.27.-i

The Gross-Pitaevskii equation (GPE) furnishes a dynamical description of superfluids and Bose-Einstein Condensates (BEC) that is valid at very low temperatures [1]. The GPE dynamics is known to produce an energy cascade that leads to a Kolmogorov regime of turbulence [2,3]. Such turbulent regimes were studied in low-temperature experiments in superfluid ^4He [4] and in BEC [5]. The truncated GPE (TGPE), obtained by performing a truncation of Fourier modes, can also describe the (classical) thermodynamic equilibrium of homogeneous BEC [6]. The TGPE (microcanonical) equilibrium is known to present (when varying the energy) a condensation transition [6,7].

In the context of classical fluids, the (conservative) truncated Euler dynamics is known to possess long-lasting transients describing dissipative phenomena [8]. With this motivation, we study in this Letter the TGPE thermalization that arises from the GPE turbulent energy cascade. Here is a short summary of our results. Partial thermalization is observed at small scales during a long transient regime; vortex lines then disappear and final thermalization sets in. A bottleneck that delays the final thermalization is characterized when large dispersive effects are present at truncation wave number.

The TGPE is obtained from the GPE describing a homogeneous BEC of volume V by truncating the Fourier transform of the wave function ψ : $\hat{\psi}_{\mathbf{k}} \equiv 0$ for $|\mathbf{k}| > k_{\max}$ [1,6]. Introducing the Galerkin projector \mathcal{P}_G that reads in Fourier space $\mathcal{P}_G[\hat{\psi}_{\mathbf{k}}] = \theta(k_{\max} - |\mathbf{k}|)\hat{\psi}_{\mathbf{k}}$ with $\theta(\cdot)$ the Heaviside function, the TGPE explicitly reads

$$i\hbar \frac{\partial \psi}{\partial t} = \mathcal{P}_G \left[-\frac{\hbar^2}{2m} \nabla^2 \psi + g \mathcal{P}_G[|\psi|^2] \psi \right], \quad (1)$$

where m is the mass of the condensed particles and $g = 4\pi\tilde{a}\hbar^2/m$, with \tilde{a} the s -wave scattering length. Madelung's transformation $\psi(\mathbf{x}, t) = \sqrt{\frac{\rho(\mathbf{x}, t)}{m}} \exp[i\frac{m}{\hbar} \phi(\mathbf{x}, t)]$ relates the

(complex) wave function ψ to a superfluid of density $\rho(\mathbf{x}, t)$ and velocity $\mathbf{v} = \nabla\phi$, where \hbar/m is the Onsager-Feynman quantum of velocity circulation around the $\psi = 0$ vortex lines [1]. When Eq. (1) is linearized around a constant $\psi = \hat{\psi}_0$, the sound velocity is given by $c = (g|\hat{\psi}_0|^2/m)^{1/2}$ with dispersive effects taking place at length scales smaller than the coherence length $\xi = (\hbar^2/2m|\hat{\psi}_0|^2g)^{1/2}$ that also corresponds to the vortex core size. In the TGPE numerical simulations presented in this Letter the density $\rho = mN/V$ is fixed to 1 and the physical constants in Eqs. (1) are determined by the values of ξk_{\max} and $c = 2$. The quantum of circulation \hbar/m has the value $c\xi/\sqrt{2}$ and $V = (2\pi)^3$.

Equation (1) exactly conserves the energy $H = \int d^3x (\frac{\hbar^2}{2m} |\nabla\psi|^2 + \frac{g}{2} [\mathcal{P}_G|\psi|^2]^2)$ and the number of particles $N = \int d^3x |\psi|^2$. Using Fourier pseudospectral methods the momentum $\mathbf{P} = \frac{\hbar}{2} \int d^3x (\psi \nabla \bar{\psi} - \bar{\psi} \nabla \psi)$ is also conserved with dealiasing performed by the 2/3-rule ($k_{\max} = 2/3 \times M/2$ [9] at resolution M).

We now study the thermalization of the superfluid Taylor-Green (TG) vortex, a flow which develops from a spatially-symmetric initial condition prepared by a minimization procedure. The TGPE integrations are performed with a dedicated pseudospectral code that uses the symmetries to speed up computations (see reference [2]). Up to 512^3 collocation points are used and the coherence length is determined by $\xi k_{\max} = 1.48$.

Vortices and density fluctuations are visualized on Fig. 1. The short time behavior, see Figs. 1(a) and 1(b), corresponds to the GPE superfluid turbulent regime previously studied in [2]. A new TGPE thermalization regime where vortices first reconnect into simpler structures and then decrease in size with the emergence of a thermal cloud is present at latter times; see Figs. 1(c) and 1(d).

To further study this relaxation dynamics, we express the energy per unit volume $E_{\text{tot}} = (H - mc^2N)/V + \frac{mc^2}{2}$ as the sum of three (space-averaged) parts [2]: the

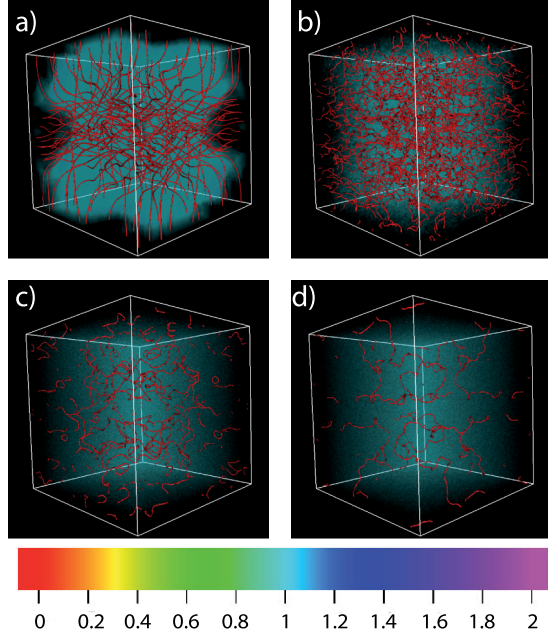


FIG. 1 (color online). 3D visualization of density at $t = 5, 10, 31$, and 55 at resolution 512^3 [see below Fig. 2(b)]. Vortices are displayed as red isosurfaces and clouds correspond to density fluctuations.

kinetic energy $E_{\text{kin}} = \langle \frac{1}{2} (\sqrt{\rho} \mathbf{v}_j)^2 \rangle$, the internal energy $E_{\text{int}} = \langle (c^2/2)(\rho - 1)^2 \rangle$ and the quantum energy $E_q = \langle c^2 \xi^2 (\partial_j \sqrt{\rho})^2 \rangle$. Parseval's theorem allows us to define corresponding energy spectra; e.g., the kinetic energy spectrum $E_{\text{kin}}(k)$ as the (solid angle integral) of $|\frac{1}{2(2\pi)^3} \times \int d^3 r e^{i\mathbf{r} \cdot \mathbf{k}_j} \sqrt{\rho} \mathbf{v}_j|^2$. $E_{\text{kin}}(k)$ can be further decomposed into compressible $E_{\text{kin}}^c(k)$ and incompressible $E_{\text{kin}}^i(k)$ parts, using $(\sqrt{\rho} \mathbf{v}_j) = (\sqrt{\rho} \mathbf{v}_j)^c + (\sqrt{\rho} \mathbf{v}_j)^i$ with $\nabla \cdot (\sqrt{\rho} \mathbf{v}_j)^i = 0$. The temporal evolution of E_{kin} , E_{kin}^i , E_{kin}^c , $E_q + E_{\text{int}}$ is displayed in Fig. 2(a) and the corresponding energy spectra in Figs. 2(c) and 2(d).

Three evolution phases are apparent on Fig. 2(a). The first phase, for $t \lesssim 15$, corresponds to the GPE regime previously studied in [2]. In the second phase, for $20 \lesssim t \lesssim 70$, the spectral convergence of the GP partial differential equation is lost and the dynamics is influenced by k_{max} . Partial thermalization starts to take place at large wave numbers where $E_{\text{kin}}(k) \sim k^2$ [see Fig. 2(c)]. Figure 2(b) shows that this phase is delayed when the resolution is increased at constant ξk_{max} . When $t > 80$ the system reaches the thermodynamic equilibrium with equipartition of energy between E_{kin}^c and $E_q + E_{\text{int}}$; see Fig. 2(d). Finally, E_{kin}^i vanishes before final thermalization [see Figs. 2(a) and 2(b)]; the total disappearance of vortices is observed on corresponding 3D visualizations (data not shown). Similar relaxation mechanisms are also present in models of hydrodynamic turbulence and the truncated Euler dynamics [8,10,11].

We now focus on a characterization of thermodynamic equilibrium that will allow us to account for the absence of

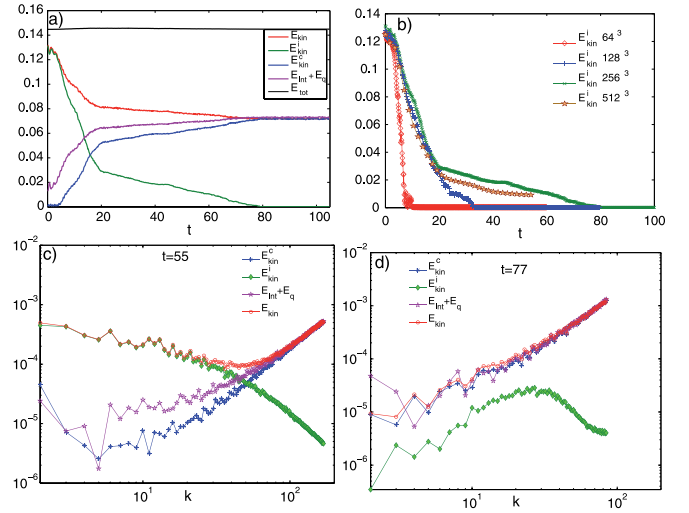


FIG. 2 (color online). (a) Temporal evolution of energies E_{kin}^c , E_{kin}^i , E_{kin} and $E_q + E_{\text{int}}$. At large times, the incompressible energy vanishes and equipartition of energy between E_{kin} and $E_q + E_{\text{int}}$ is observed. Resolution of 256^3 . (b) Temporal evolution of E_{kin}^i at resolution of 64^3 , 128^3 , 256^3 and 512^3 with constant $\xi k_{\text{max}} = 1.48$. (c)–(d) Energy spectra at $t = 55$ and $t = 77$ resolution 512^3 and 256^3 , respectively.

vortices and the equipartition of energy in the final states. Microcanonical equilibrium states are known to result from long-time integration of TGPE [6,7]. Grand canonical equilibrium states are given by the probability distribution $\mathbb{P}_{\text{st}}[\psi] = Z^{-1} \exp[-\beta(H - \mu N)]$. They allow us to directly control the temperature (instead of the energy in a microcanonical framework). These states can be efficiently obtained by constructing a stochastic process that converges to a realization with the probability $\mathbb{P}_{\text{st}}[\psi]$ [12]. This process is defined by a Langevin equation consisting in a stochastic Ginzburg-Landau equation (SGLE):

$$\hbar \frac{\partial \psi}{\partial t} = \mathcal{P}_G \left[\frac{\hbar^2}{2m} \nabla^2 \psi + \mu \psi - g \mathcal{P}_G[|\psi|^2] \psi \right] + \sqrt{\frac{2\hbar}{V\beta}} \mathcal{P}_G[\zeta(\mathbf{x}, t)], \quad (2)$$

where the white noise $\zeta(\mathbf{x}, t)$ satisfies $\langle \zeta(\mathbf{x}, t) \zeta^*(\mathbf{x}', t') \rangle = \delta(t - t') \delta(\mathbf{x} - \mathbf{x}')$, β is the inverse temperature and μ the chemical potential. Using this algorithm in [12] the microcanonical and grand canonical ensembles were shown to be equivalent and the condensation transition reported in [6,7] identified with the standard second order λ transition (see insets on Fig. 3). Note that c_p would be very difficult to obtain from microcanonical results.

At low temperature the partition function Z can be exactly computed by the steepest-descent method [12]. In particular, the mean value of the condensate amplitude reads $|\hat{\psi}_0|^2 = \frac{\mu}{g} - \frac{\mathcal{N}}{V\beta\mu} f_0[\frac{4m\mu}{\hbar^2 k_{\text{max}}^2}]$, where $\mathcal{N} = k_{\text{max}}^3 V / 6\pi^2$ is the total number of modes and $f_0[z] = 3z - 9z^{3/2} \cot^{-1}(\sqrt{z})/4$.

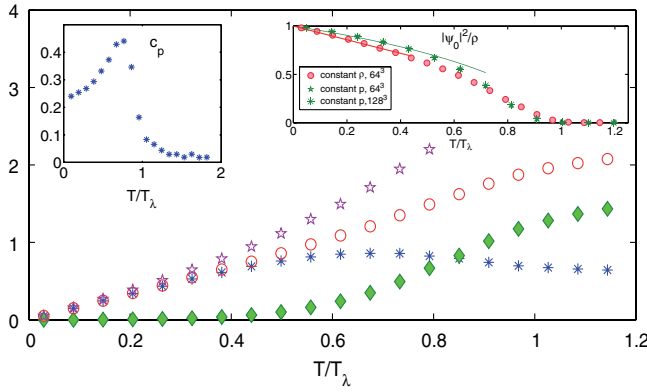


FIG. 3 (color online). Temperature dependence of the energies E_{kin}^c (stars), E_{kin}^i (diamonds), E_{kin}^q (circles) and $E_q + E_{\text{int}}$ (pentagrams) at constant density. Insets: (right) Temperature dependence of the condensate fraction $|\psi_0|^2/\rho$; (left) Specific heat $c_p = \frac{\partial H}{\partial T}|_p$ at resolution 128^3 .

In numerical simulations of Eq. (2), μ is adjusted to fix the density (or the pressure p) [12]. The inverse temperature is normalized as $\beta = \mathcal{N}/VT$. With this choice of parametrization the λ -transition temperature T_λ is independent of \mathcal{N} . Data from SGLE and low-temperature calculation are confronted on Fig. 3 and seen to be in good agreement.

The temperature dependence of the different energies is displayed on Fig. 3. Observe that E_{kin}^i vanishes at temperatures $T/T_\lambda \lesssim 1/2$. This explains the disappearance of vortices in Fig. 2 above as the corresponding final temperature is well below T_λ [see corresponding values of energies on Fig. 2(a)]. At low-temperature equipartition of energy between E_{kin} and $E_q + E_{\text{int}}$ is also apparent on Fig. 3. Note that a larger k_{max} implies, by equipartition, a lower temperature. The corresponding dissipative effects are thus smaller explaining the thermalization delay apparent on Fig. 2(b).

We now turn to the study of dispersive effects on the thermalization of the TGPE dynamics. In order to investigate dispersive effects, the TG initial condition described above is prepared at fixed $\xi = \sqrt{2}/20$ and varying resolution: 64^3 , 128^3 , and 256^3 . The three initial condition thus represent the same field at different resolutions.

The evolutions of the energies of the three runs are shown on Fig. 4(a). They are identical until $t \approx 5$ where the run at resolution 64^3 starts to lose spectral convergence. All runs appear to have completely thermalized at $t \approx 20$. However the kinetic energy spectra corresponding to this time, displayed on Fig. 4(b), shows clear differences between runs. The high-wave number modes are thermalized in the 64^3 run but they decay at large k at higher resolutions. In the 256^3 run, two zones are clearly distinguished: an intermediate thermalized range (with approximative k^2 scaling) followed, well before $k_{\text{max}} = 85$, by a steep decay zone.

The temporal evolution of $E_{\text{kin}}(k)$ for the 256^3 run displayed in Fig. 4(c) is well represented by a fit of the form

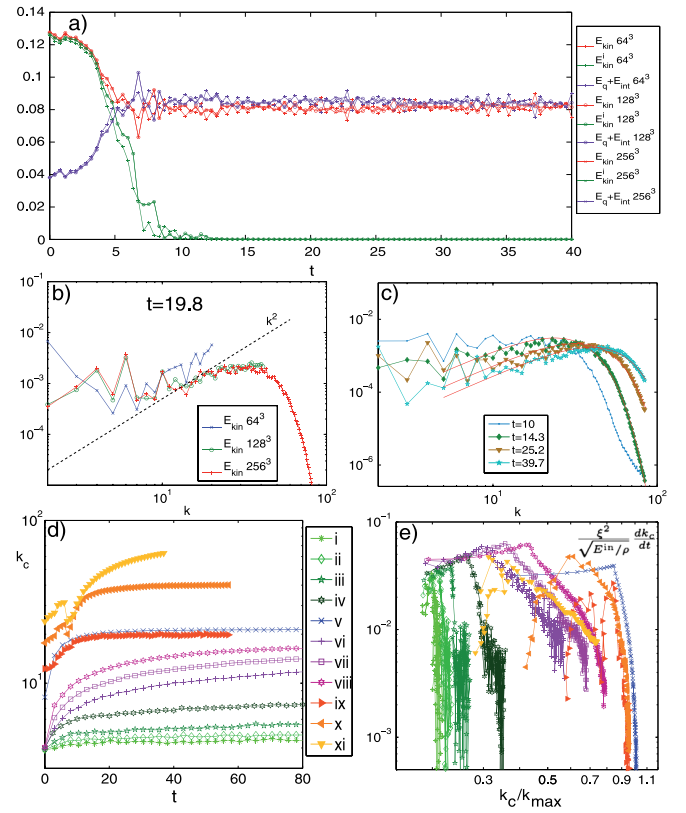


FIG. 4 (color online). (a) Evolution of energies at $\xi = \sqrt{2}/20$ and resolution 64^3 , 128^3 , and 256^3 . (b) Energy spectrum $E_{\text{kin}}(k)$ at $t = 19.8$ for the three TG runs. (c) Evolution of $E_{\text{kin}}(k)$, solid red lines are fits of the form $Ak^2 \exp[-\gamma^2 k^2]$ (see text). (d) Evolution of k_c . Curves i–iv: $\xi = 2\sqrt{2}/5$, $k_c^{\text{in}} = 4$, $E^{\text{in}} = 0.1, 0.2, 0.4, 1$; v: $\xi = \sqrt{2}/10$, $k_c^{\text{in}} = 8$, $E^{\text{in}} = 0.2$; vi–viii: $\xi = \sqrt{2}/5$, $E^{\text{in}} = 0.1, 0.2, 0.4$ [(i)–(viii)] in resolution 64^3 ; ix–xi: Taylor-Green resolutions 64^3 , 128^3 , and 256^3 . (e) Parametric representation dk_c/dt vs k_c/k_{max} (same labels as d).

$A(t)k^2 \exp[-\gamma^2(t)k^2]$, where $A(t)$ and $k_c(t) \sim \gamma^{-1}(t) \ll k_{\text{max}}$ are increasing functions of t . Such a behavior of the energy spectra ensures spectral convergence and the dynamics is thus not influenced by k_{max} . Furthermore, we checked that $A(t)k_c^3(t) \approx E_{\text{kin}}$ for $t \gtrsim 20$ (data not shown). This new regime can be described as a (quasi) thermalization, with self-truncation at wave number k_c and temperature $T \sim E/k_c^3$, that spontaneously establishes itself within the GP partial differential equation dynamics when the direct energy cascade is inhibited by a dispersive bottleneck for the energy transfer [13].

An open question is whether thermalization is simply delayed or, as in the Fermi-Pasta-Ulam-Tsingu problem [15], completely inhibited in the self-truncation regime $\xi k_{\text{max}} \rightarrow \infty$. It is not feasible now to directly study this limit, within the TG framework, as it requires long runs at arbitrarily high resolution. To skip the TG cascade regime and directly study the self-truncated thermalization regime we use initial data generated by the SGLE instead of the TG vortex. To wit, we use Eq. (2) with a variable truncation wave number k_c^{in} , set to a target value of k_c , smaller than

the maximum truncation wave number k_{\max} allowed by the resolution. This SGLE-generated initial data is then used to run the TGPE at a given value of ξk_c with arbitrarily large values of ξk_{\max} .

A number of such runs were performed at resolution 64^3 with various values of k_c^{in} , ξ , and initial energy E^{in} . The result of these computations are compared with the TG runs and displayed on Fig. 4(d). The self-truncation wave number is explicitly determined from E_{kin} by the integral formula $k_c^2 = \frac{5}{3} \int_0^{k_{\max}} k^2 E_{\text{kin}}(k) dk / \int_0^{k_{\max}} E_{\text{kin}}(k) dk$. A general growth in time of k_c is apparent on Fig. 4(d) for both the Taylor-Green runs and the SGLE-generated initial data, showing similar behavior.

In order to check for a self-similar regime a parametric log-log representation of dk_c/dt vs k_c is used on Fig. 4(e). With this representation, a self-similar evolution $k_c(t) \sim t^\alpha$ corresponds to a line of slope $(\alpha - 1)/\alpha$. Figure 4(e) shows transient self-similar evolutions terminated by a vertical asymptote corresponding to logarithmic growth ($\alpha = 0$). This self-truncation takes place at small values of k_c/k_{\max} strongly suggesting that the self-truncation happens in a regime independent of cutoff. This regime should, in principle, be amenable to a description in terms of wave turbulence theory along the lines of reference [16].

Let us concentrate now on estimations of order of magnitude relevant to physical weakly-interacting BEC. At very low temperature, the GPE gives an accurate description of the (classical) dynamics of BEC [1] at scales larger than the mean interatomic particle distance $\ell \sim |\hat{\psi}_0|^{-2/3}$, satisfying $\tilde{a} \ll \ell \ll \xi$. At finite temperature [1,6], Bogoliubov's dispersion relation $\omega_B^2(k) = k^2 g |\psi_0|^2/m + k^4 \hbar^2/4m$ and the relation $\hbar \omega_B(k_{\text{eq}}) = \beta^{-1} = k_B T$ imply that phonons are in equipartition only for wave numbers $k < k_{\text{eq}}$. The equipartition wave number thus satisfies $\xi k_{\text{eq}} \sim T/T^*$ for $T \ll T^*$ and $\xi k_{\text{eq}} \sim \sqrt{T/T^*}$ for $T \gg T^*$, with $T^* = \ell^2 T_\lambda / \xi^2$ and $T_\lambda \sim \hbar^2/k_B m \ell^2$ the condensation temperature (see Ref. [1]). Thus physical BEC at low-temperature have a natural cutoff for the equipartition range given by $k_{\max} = k_{\text{eq}}(T)$.

In experimental BEC the value of ξk_{eq} is large because $T^*/T_\lambda \sim \ell^2/\xi^2 \ll 1$ and the corresponding TGPE has a large ξk_{\max} . This strongly suggests that, unless overwhelmed by other (non-TGPE) relaxation mechanisms, the thermalization slowdown caused by the dispersive bottleneck should be observable. It would thus be interesting to investigate in the future the suppression of aspect-ratio inversion observed in recent turbulent BEC experiments [5] in the context of the TGPE in a nonhomogeneous trapping geometry.

In the context of classical hydrodynamics, self-truncation can take place in fluids with dispersion, e.g., MHD flows with Alfvén waves [12]. Models of turbulence of the Euler- α [17] type, where the right-hand side of the incompressible Euler equation is multiplied by the operator $(1 - \alpha \nabla^2)^{-1}$ that penalizes the energy at small scales, are also plausible candidates for self-truncation.

In summary we investigated the thermalization dynamics in turbulent BEC using the TGPE. Our main result is that a bottleneck delays the final thermalization when large dispersive effects are present at truncation wave number and produces an effective self-truncation. These effects are in principle observable in physical BEC.

We acknowledge useful scientific discussions with G. Düring and S. Rica. The computations were carried out at IDRIS (CNRS) and visualizations used VAPOR [18].

-
- [1] N.P. Proukakis and B. Jackson, *J. Phys. B* **41**, 203002 (2008).
 - [2] C. Nore, M. Abid, and M.E. Brachet, *Phys. Rev. Lett.* **78**, 3896 (1997); C. Nore, M. Abid, and M.E. Brachet, *Phys. Fluids* **9**, 2644 (1997).
 - [3] M. Kobayashi and M. Tsubota, *Phys. Rev. Lett.* **94**, 065302 (2005).
 - [4] J. Maurer and P. Tabeling, *Europhys. Lett.* **43**, 29 (1998).
 - [5] E.A.L. Henn *et al.*, *Phys. Rev. Lett.* **103**, 045301 (2009).
 - [6] M. J. Davis, S. A. Morgan, and K. Burnett, *Phys. Rev. Lett.* **87**, 160402 (2001).
 - [7] C. Connaughton *et al.*, *Phys. Rev. Lett.* **95**, 263901 (2005); A. Picozzi, G. Düring, and S. Rica, *Physica (Amsterdam)* **238D**, 1524 (2009).
 - [8] C. Cichowlas *et al.*, *Phys. Rev. Lett.* **95**, 264502 (2005).
 - [9] D. Gottlieb and S.A. Orszag, *Numerical Analysis of Spectral Methods* (SIAM, Philadelphia, 1977).
 - [10] C. Connaughton and S. Nazarenko, *Phys. Rev. Lett.* **92**, 044501 (2004).
 - [11] U. Frisch *et al.*, *Phys. Rev. Lett.* **101**, 144501 (2008).
 - [12] G. Krstulovic, Ph.D. thesis, Université Paris VI, 2010, <http://tel.archives-ouvertes.fr/tel-00505813/fr/>; G. Krstulovic and M.E. Brachet (to be published).
 - [13] A different kind of bottleneck was proposed in [14], with a inhibition of the energy transfer involving Kelvin wave cascading along vortices rather than dispersive effects.
 - [14] V. S. L'vov, S. V. Nazarenko, and O. Rudenko, *Phys. Rev. B* **76**, 024520 (2007).
 - [15] E. Fermi, J. Pasta, and S. Ulam, LASL Report No. LA-1940, 1955.
 - [16] B. V. Svistunov *J. Mosc. Phys. Soc.* **1**, 373 (1991).
 - [17] J. Linshiz and E. Titi, *J. Stat. Phys.* **138**, 305 (2010).
 - [18] <http://www.vapor.ucar.edu>.